Supplementary Information

High Temperature Thermal and Melting Properties of Uranium-Neptunium and Plutonium-Neptunium Mixed Oxides: A MD Simulation Study

A. Chakraborty,[†,‡] N. Choudhury,[*,¶,‡] and P. S. Ghosh[*,§,‡]

†*Reactor Physics Design Division, Bhabha Atomic Research Center, Mumbai 400 085, India*

‡*Homi Bhabha National Institute, Anushaktinagar, Mumbai 400 094, India*

¶*Chemistry Division, Bhabha Atomic Research Center, Mumbai 400 085, India*

§*Glass & Advanced Materials Division, Bhabha Atomic Research Center, Mumbai 400 085, India*

E-mail: nihcho@barc.gov.in; psghosh@barc.gov.in

Interatomic Potential Parameters

Table S1: Parameters for pair interaction and the many-body interactions, in bold, the terms re-optimized in this study.

Species α	Species β	$A_{\alpha\beta}$ (eV)	$\rho_{\alpha\beta}$ $(\AA)$	$C_{\alpha\beta}$ $(eV\AA^6)$	$D_{\alpha\beta}$ (eV)	$\gamma_{\alpha\beta}$ $(\AA^{-1})$	$r^0_{\alpha\beta}$ $(\AA)$	Reference
U^{4+}	U^{4+}	18600	0.2747	0.0	-	-	-	[1]
U^{5+}	U^{5+}	18600	0.2429	0.0	-	-	-	[2]
Np^{4+}	Np^{4+}	18600	0.2692	0.0	-	-	-	[1]
Pu^{3+}	Pu^{3+}	18600	0.2761	0.0	-	-	-	[3]
Pu^{4+}	Pu^{4+}	18600	0.2637	0.0	-	-	-	[1]
U^{4+}	U^{5+}	18600	0.258290	0.0	-	-	-	[2]
U^{4+}	Np^{4+}	18600	0.271936	0.0	-	-	-	[1]
U^{4+}	Pu^{3+}	18600	0.256700	0.0	-	-	-	-
U^{4+}	Pu^{4+}	18600	0.269144	0.0	-	-	-	[1]
U^{5+}	Np^{4+}	18600	0.255696	0.0	-	-	-	-
U^{5+}	Pu^{3+}	18600	0.258953	0.0	-	-	-	-
U^{5+}	Pu^{4+}	18600	0.253071	0.0	-	-	-	-
Np^{4+}	Pu^{3+}	18600	0.272628	0.0	-	-	-	-
Np^{4+}	Pu^{4+}	18600	0.266436	0.0	-	-	-	[1]
Pu^{3+}	Pu^{4+}	18600	0.269829	0.0	-	-	-	[3]
U^{4+}	O	448.779	0.387758	0.0	0.66080	2.05815	2.38051	[1]
U^{5+}	O	1155.631	0.346480	0.0	1.93170	1.4881	2.07090	[2]
Np^{4+}	O	**360.376**	**0.4189**	0.0	**0.8659**	**1.876**	2.368	this work
Pu^{3+}	O	527.5159	0.384200	0.0	0.70185	1.98008	2.40840	[3]
Pu^{4+}	O	527.5159	0.379344	0.0	0.70185	1.98008	2.34591	[1]
O	O	830.283	0.3529	3.8843	-	-	-	[1]

Species	G_α $(eV\AA^{1.5})$	n_β $(\AA^5)$	Reference
U^{4+}	1.806	3450.995	[1]
U^{5+}	1.806	3450.995	[2]
Np^{4+}	**1.4346**	**3980.058**	this work
Pu^{3+}	2.168	3980.058	[3]
Pu^{4+}	2.168	3980.058	[1]
O	0.690	106.856	[1]

Lattice Parameter

The parameters obtained from the fitting of the present MD simulation data for the lattice parameters ($a(T)$) vs. T in the temperature range of 300-1300 K using a cubic equation as

given in Eq. (4) of the main text are listed below:

Table S2: Parameters of the polynomial for lattice parameter of $U_{1-y}Np_yO_2$ and $Pu_{1-y}Np_yO_2$ described by equation 4 in the temperature range of 300 K to 1300 K. The coefficients of the equation are compared with experimental high-temperature XRD-fitted values for end members. MD calculated values of $a(300)$ and linear thermal expansion coefficients (LTE) determined from equation 4 are also compared with experiments.

y	b_0	$b_1(10^{-5})$	$b_2(10^{-9})$	$b_3(10^{-12})$	$a(300)(\AA)$	$LTE(10^{-6}K^{-1})$
$U_{1-y}Np_yO_2$						
0.0000	5.45332	5.13334	4.02624	1.24895	5.46912	11.06028
0.1250	5.44653	5.07574	4.03447	1.21812	5.46216	10.94439
0.2500	5.44024	5.11978	2.76436	1.68995	5.45588	10.87084
0.3125	5.43752	5.06672	3.28616	1.40266	5.45307	10.81226
0.5000	5.42989	5.07334	2.29113	1.78009	5.44536	10.68800
0.6875	5.42386	4.95526	3.21967	1.24887	5.43905	10.55147
0.7500	5.42213	4.89743	3.86914	0.90233	5.43718	10.52384
1.0000	5.41623	4.82873	3.71434	0.87779	5.43106	10.33868
HT XRD					(at 298 K)	
0.0[4]	5.45567	4.581	10.36	-2.736	5.4702	10.31180
0.1[4]	5.45203	4.193	13.82	-3.872	5.4667	9.98388
0.3[4]	5.44396	3.878	16.15	-4.365	5.4568	10.10982
0.5[4]	5.43903	3.468	21.11	-6.028	5.4511	10.15129
0.7[4]	5.43245	3.462	20.63	-5.925	5.4445	10.04575
1.0[4]	5.42032	4.276	9.075	-1.362	5.4338	10.00106
$Pu_{1-y}Np_yO_2$						
0.0000	5.37986	5.08986	3.18514	1.71882	5.39547	11.06854
0.0625	5.38141	4.94090	5.00709	0.82029	5.39673	10.97887
0.1250	5.38267	5.01519	3.27910	1.61978	5.39806	10.90021
0.1875	5.38426	4.99679	3.35799	1.43315	5.39959	10.82860
0.2500	5.38599	4.96163	3.64959	1.19484	5.40124	10.75679
0.5000	5.39414	4.93314	2.79284	1.53570	5.40923	10.57822
0.7500	5.40434	4.85936	3.39487	1.14206	5.41926	10.42393
1.0000	5.41623	4.82873	3.71434	0.87779	5.43106	10.33868
HT XRD					(at 298 K)	
0.0[5]	5.38397	3.169	23.59	-6.265	5.3953	10.35312
0.05[5]	5.38534	3.395	20.67	-5.137	5.3972	10.34049
0.10[5]	5.38793	3.178	23.95	-6.693	5.3994	10.27966
0.20[5]	5.39163	3.202	24.20	-6.993	5.4031	10.28654
0.50[5]	5.40328	3.551	18.54	-4.373	5.4154	10.27751

Enthalpy Increment

The coefficients obtained from the fitting of the enthalpy increment (ΔH versus T) data obtained from the present MD simulations using the Mayer-Kelley polynomial relation (see Eq. (5) of the main text) are as follows:

Table S3: Parameters for the fit of the enthalpy increment of $U_{1-y}Np_xO_2$ and $Pu_{1-y}Np_yO_2$ described by equations 5 in the temperature range of 300 K to 2000 K

y	a $(kJ.mol^{-1})$	$b(\times 10^{-2})$ $(kJ.mol^{-1}.K^{-1})$	$c(\times 10^{-6})$ $(kJ.mol^{-1}.K^{-2})$	$d(\times 10^{2})$ $(kJ.mol^{-1}.K)$
$U_{1-y}Np_yO_2$				
0.0000	-20.61333	7.12764	4.12488	-3.42074
0.0625	-20.47562	7.10827	4.17844	-3.69142
0.1250	-20.62541	7.12258	4.11039	-3.40591
0.1875	-20.64062	7.12922	4.04878	-3.47221
0.2500	-20.57563	7.12253	4.06655	-3.46484
0.3125	-20.63270	7.12526	4.04855	-3.41797
0.5000	-20.30953	7.09083	4.11406	-3.96373
0.6875	-20.60301	7.12894	3.93261	-3.41478
0.7500	-20.43915	7.10471	4.01211	-3.76544
0.8125	-20.50548	7.11459	3.97040	-3.56681
0.8750	-20.62479	7.13052	3.89581	-3.39628
0.9375	-20.71210	7.13867	3.84993	-3.25920
1.0000	-20.48573	7.11318	3.94539	-3.69235
$Pu_{1-y}Np_yO_2$				
0.0000	-20.27719	7.06498	4.42716	-4.02806
0.0625	-20.08875	7.04005	4.49754	-4.43945
0.1250	-20.63342	7.11591	4.20219	-3.26078
0.1875	-20.16287	7.05999	4.34928	-4.26411
0.2500	-19.92925	7.02215	4.48591	-4.69994
0.3125	-20.45666	7.10557	4.13798	-3.70644
0.5000	-20.49184	7.10396	4.09955	-3.60921
0.6875	-20.35108	7.09466	4.07094	-3.89597
0.7500	-20.48298	7.10743	4.01626	-3.68243
0.8125	-20.40823	7.10868	3.97806	-3.75005
0.8750	-20.59821	7.12690	3.90259	-3.50324
0.9375	-20.55368	7.11688	3.94535	-3.51418
1.0000	-20.48573	7.11318	3.94539	-3.69235

Specific Heat Capacity

The parameters obtained from the fitting of the specific heat capacity vs. T data obtained from the present MD simulation in the temperature range of 300-2000 K with Eq. (6) of the main text are listed below:

Table S4: Specific heat capacity at 300 K and parameters for the fit of the high-temperature specific heat capacity of $U_{1-y}Np_yO_2$ and $Pu_{1-y}Np_yO_2$ described by equations 6 in the temperature range of 300 K to 2000 K

y	$C_p(300K)$ $(J.mol^{-1}.K^{-1})$	a $(J.mol^{-1}.K^{-1})$	$b(\times10^{-3})$ $(J.mol^{-1}.K^{-2})$	$c(\times10^{6})$ $(J.mol^{-1}.K)$
$U_{1-y}Np_yO_2$				
0.0000	76.04504	71.68273	8.20853	0.18448
0.0625	76.16503	71.54227	8.27889	0.20450
0.1250	75.96177	71.74378	8.07870	0.17425
0.1875	75.96563	71.68835	8.08478	0.18158
0.2500	75.87564	71.66210	8.08549	0.17698
0.3125	75.98654	71.77783	7.94402	0.17694
0.5000	76.07666	71.42188	8.13187	0.21340
0.6875	76.02948	71.44697	8.03808	0.20889
0.7500	75.92954	71.50345	7.97886	0.19811
0.8125	75.99999	71.30093	8.13504	0.21772
0.8750	75.99638	71.35869	8.06214	0.21479
0.9375	75.97360	71.48005	7.91936	0.20448
1.0000	75.95568	71.20942	8.18479	0.22303
HT experiment				
1.0	66.22[4]	81.30[6]	7.062[6]	-2.117[6]
$Pu_{1-y}Np_yO_2$				
0.0000	76.01928	70.51934	9.36978	0.26318
0.0625	75.96700	70.72076	9.15083	0.24543
0.1250	75.84415	70.92096	8.94590	0.22029
0.1875	76.12744	70.75375	8.96439	0.25980
0.2500	76.05152	70.59033	9.09250	0.26576
0.3125	76.12059	71.08356	8.59997	0.23730
0.5000	75.96974	71.12306	8.46702	0.22375
0.6875	76.08612	71.09016	8.37652	0.24031
0.7500	75.86681	71.20691	8.28434	0.21381
0.8125	76.03695	71.06132	8.33824	0.24099
0.8750	76.04691	71.42113	7.99412	0.21476
0.9375	75.94037	71.33361	8.07295	0.21120
1.0000	75.95568	71.20942	8.18479	0.22303
HT experiment				
0.0[7]	17.32	22.18	2.080	-0.4935
1.0	66.22[4]	81.30[6]	7.062[6]	-2.117[6]

Thermal Expansion Coefficient (α) and Specific Heat Capacity

The parameters obtained from the fitting of the specific heat capacity as well as Thermal (volume) expansion coefficient (α) data as a function of temperature (T) obtained from the present MD simulations by a common set of equations (Eq. (10)-(13) of the main text) are listed below:

Table S5: The parameters obtained by fitting MD calculated thermal expansion coefficient (α) and specific heat (C_p) data for $U_{1-y}Np_yO_2$ MOX and $Pu_{1-y}Np_yO_2$ MOX using the equations (10)-(13).

Parameters	α		C_p	
	$U_{1-y}Np_yO_2$	$Pu_{1-y}Np_yO_2$	$U_{1-y}Np_yO_2$	$Pu_{1-y}Np_yO_2$
A $(Jmol^{-1}K^{-1})$	4.50642×10^{-5}	38.87594	5.15588×10^{5}	858.669
A_0 $(Jmol^{-1}K^{-1})$	1.96282×10^{-5}	4.55491×10^{-5}	3.01873×10^{4}	91.650
A_1 (K)	2781.164	3672.604	2469.909	2698.928
A_2 (K)	2534.171	2274.876	4022.018	2163.326
A_3 (K)	2338.799	452.916	2706.784	2407.244
B_1 (K)	330.709	2.900	197.615	274.596
B_2 (K)	281.463	458.620	16.480	235.376
B_3 (K)	440.317	542.932	218.773	243.111
W_1 (K)	0	0	0	0
W_2 (K)	-64.901	234.860	1.176	30.234
W_3 (K)	0	0	0	0
P_{HL} $(Jmol^{-1}K^{-1})$	1.63654×10^{-4}	-24.804	2.69568×10^{5}	111.226
P_{ML} (K)	246.592	109.539	235.344	-73.916
σ_1 (K)	224.351	282.629	7.16802×10^{5}	190.836
σ_2 (K)	1454.204	131.803	-2.48336×10^{8}	-187.012
σ_3 (K)	2067.236	1361.828	3.97803×10^{9}	1354.165
μ_1 (K)	2609.953	2562.064	-352.414	3036.655
μ_2 (K)	3265.411	2305.960	1.65232×10^{9}	2405.035
g_1 $(Jmol^{-1})$	2.33289×10^{-3}	-5.10060×10^{-3}	-5.41054×10^{9}	5921.732
g_2 $(Jmol^{-1})$	0.118	7.97404×10^{-3}	9.89278×10^{9}	6.82833×10^{4}
g_3 $(Jmol^{-1})$	2.9×10^{-2}	-6.14974×10^{-2}	1204.252	-5.37784×10^{4}
P_{MG} (K)	-271.843	45.067	608.997	68.237
P_{HG} $(Jmol^{-1})$	5.12062	-1.03449×10^{-3}	-5.56727×10^{5}	2272.246

Component-wise Analysis of Heat Capacity

The theoretical model of heat capacity for actinide oxides is complex due to various contributing mechanisms other than simple lattice vibrations. These models typically aim to account for different physical processes that contribute to heat capacity, especially at high temperatures. Heat capacity of oxides at constant pressure and constant volume can be expressed using equation S1

$$\begin{aligned} C_p &= C_l + C_{sch} + C_d + C_{exe} \\ C_v &= C_l + C_{sch} + C_{exe} \end{aligned} \tag{S1}$$

Where C_l, C_{sch}, C_d, and C_{exe} are components of the heat capacity due to the lattice, Schottky-type, dilatational, and defect, respectively.

(a) Lattice heat capacity

The heat capacity estimation from lattice vibration can be calculated on the basis of the Debye model. It is based on the harmonic lattice vibration given by equation S2.

$$C_l = 9nR\left(\frac{T}{\Theta_D}\right)^3 \int_0^{\Theta_D/T} \frac{x^4 e^x}{(e^x-1)^2} dx \tag{S2}$$

Where n is the number of atoms in a molecule, R is the universal gas constant, and Θ_D is the Debye temperature. The Debye temperature for different actinide oxides is tabulated in Table S6 obtained from the literature.

Table S6: Grüneisen constant and Debye temperature of different actinide oxides

Compositions	γ	Θ_D (K)
UO_2	1.7[8]	377[8]
PuO_2	2.6[8]	415[8]
NpO_2	1.93 ± 0.03[8]	435 ± 2[8]

(b) Schottky heat capacity

The Schottky heat capacity arises from the thermal excitation of localized 5f-electrons.[9] The Helmholtz energy per cation can be expressed as

$$F = U - TS = -kT \ln Z \tag{S3}$$

$$Z = \sum_i g_i e^{-\frac{E_i}{kT}} \tag{S4}$$

Where Z is the partition function, E_i is the energy levels of 5f electrons, and g_i is their degeneracies. The Shottky heat capacity can be written as

$$C_{sch} = T\frac{\partial^2 F}{\partial T^2} \tag{S5}$$

Kato et al.[10] reported C_{sch} of actinide oxides using equation S6. The parameters in this equation are given in Table S7.

$$C_{sch} = nR\frac{(\frac{\epsilon_1}{RT})^2 g_1 g_0 e^{-\epsilon_1/RT} + (\frac{\epsilon_2}{RT})^2 g_2 g_0 e^{-\epsilon_2/RT} + (\frac{\epsilon_1+\epsilon_2}{RT})^2 g_1 g_2 e^{-(\epsilon_1+\epsilon_2)/RT} + (\frac{\epsilon_1+\epsilon_2}{RT})^2 g_2 g_1 e^{-(\epsilon_1+\epsilon_2)/RT}}{(g_0 + g_1 e^{-\epsilon_1/RT} + g_2 e^{-\epsilon_2/RT} + g_1 g_2 e^{-(\epsilon_1+\epsilon_2)/RT})^2} \tag{S6}$$

Table S7: The parameters corresponding to different actinide oxides for equation S6[10]

	UO_2	PuO_2	NpO_2
$g1/g0$	0.1	0.1	0.26058
$g2/g0$	0.9	1.25	0.062192
$g3/g0$	–	0	0.62836
e_1	2112.4	2534.9	3343.2
e_2	25349.0	21969.1	22079.6
e_3	–	–	87188.6

(c) Dilatational heat capacity

The Dilatational heat capacity arises due to anharmonic effects cause phonon frequencies to vary with temperature, necessitating corrections to the harmonic models. This term consists of Grüneisen parameter (γ) and thermal expansion (α) as shown in eq S7

$$C_d = C_V \gamma \alpha T \tag{S7}$$

where γ is Grüneisen constant expressed by eq S8 and the volumetric thermal expansion coefficient α is given by equation S9. The values of γ and the coefficient of LTE are given in Table S6 and Table S8, respectively.

$$\gamma = \alpha K V_m / C_V \tag{S8}$$

$$\begin{aligned} LTE &= \frac{1}{L}\left(\frac{dL}{dT}\right)_p = a_0 + a_1 T + a_2 T^2 + a_3 T^3 \\ \alpha &= 3LTE \end{aligned} \tag{S9}$$

Table S8: The coefficient of LTE corresponding to different actinide oxides given by equation S9[10]

	UO_2	PuO_2	NpO_2
$a0$ $(\times 10^{-03})$	-2.8809	-2.8350	-2.8800
$a1$ $(\times 10^{-06})$	9.5024	9.2931	9.4456
$a2$ $(\times 10^{-10})$	2.0894	4.0022	4.7621
$a3$ $(\times 10^{-13})$	4.4096	3.0084	-

(d) Excess heat capacity

At very high temperatures (e.g., above 1000 K), an additional, often significant, contribution to heat capacity arises from thermally induced disorder, such as the formation of oxygen Frenkel pairs and the formation of polarons. This is sometimes referred to as excess heat

capacity (C_{exe}). The defect concentration (x)[11] in the lattice is described by statistical mechanics, relating it to the enthalpy (ΔH_{def}) and entropy (ΔS_{def}) of formation shown in equation S10. The corresponding excess heat capacity (C_{exe}) is then calculated from the temperature derivative of $x\Delta H_{def}$ given by equation S11.

$$x = \sqrt{2}exp\left(\frac{-\Delta G_{def}}{2RT}\right) = \sqrt{2}exp\left(\frac{-\Delta H_{def}}{2RT}\right)exp\left(\frac{\Delta S_{def}}{2R}\right) \tag{S10}$$

$$C_{exe} = \frac{d}{dT}\Delta H_{enthalpy} = \frac{d}{dT}x\Delta H_{def} \tag{S11}$$

The derivative properties, such as the heat capacity at constant pressure of actinide oxides, show a second-order transition at a critical temperature (T_λ) below the melting temperature. It is generally called the Bredig transition. To accommodate the phenomena in the model, Kato et al.[10] proposed the new function to express the defect concentration shown in equation S12.

$$x = \left[x_1^{-5} + x_2^{-5}\right]^{-1/5} \tag{S12}$$

where x_1 and x_2 are shown in equation S13.

$$\begin{aligned} x_1 &= exp\left(\frac{-\Delta H_1}{2RT}\right)exp\left(\frac{\Delta S_1}{2R}\right) \\ x_2 &= exp\left(\frac{-\Delta H_2}{2RT}\right)exp\left(\frac{\Delta S_2}{2R}\right) \end{aligned} \tag{S13}$$

Here, ΔH_1 and ΔS_1 represent the enthalpy and entropy of defect formation below the Bredig transition temperature (T_λ), while ΔH_2 and ΔS_2 denote the enthalpy and entropy of defect formation above the Bredig transition temperature. Kato et al.[10] proposed that the enthalpy decreases by a factor of three following the Bredig transition. They provided the values for UO_2 and PuO_2. The enthalpies and entropies of defect formation in NpO_2 are

estimated as a function of the An–O atomic distance in the AnO_2 compounds, following the approach adopted by Koning et al.[11] The values of ΔH_2 and ΔS_2 for different actinide oxides are tabulated in Table S9. Substituting the new defect concentration in equation S11 yields the heat capacity due to defect formation given by equation S14. In the present calculation, the ΔH in equation S14 is approximated as ΔH_1.

$$C_{exe} = \frac{\Delta H}{2RT^2} \frac{1}{[x_1 + x_2]^{6/5}} [\Delta H_1 x_1 + \Delta H_2 x_2] \tag{S14}$$

Table S9: Thermodynamic properties of different actinide oxides

Compositions	Below Bredig transition		Above Bredig transition		Bredig transition temperature (K)
	ΔH_i $(kJmol^{-1})$	ΔS_i $(JK^{-1}mol^{-1})$	ΔH_i $(kJmol^{-1})$	ΔS_i $(JK^{-1}mol^{-1})$	
UO_2	300[10]	85[10]	100	14	2689
PuO_2	350[10]	105[10]	116	17	2571
NpO_2	325	95	108	15	2609

The defect concentrations x_1 and x_2 for UO_2, PuO_2, and NpO_2 are plotted as a function of $\frac{1}{T}$ as shown in Fig. S1. The total defect concentration x is shown as a dotted line. Now, the total heat capacity can be obtained using equation S1. The components of the heat capacity for UO_2, PuO_2, and NpO_2 are plotted as a function of temperature, as shown in Fig. S2. The Bredig transition temperatures of all pure actinide oxides are tabulated in Table S9. The heat capacity at constant pressure (C_p) for all three pure actinide oxides estimated from the model is compared in Fig. S3.The heat capacity of MOX system can be estimated using weighted average of all the components (C_l, C_{sch}, C_d, C_{exe}) of heat capacities of its constituent oxides. This approach assumes that the total heat capacity of the MOX fuel is a linear combination of the heat capacities of each component, weighted by their respective molar or mass fractions. The overall heat capacity of the MOX fuel at temperature T is calculated as

$$C_p^{MOX} = x_{UO_2} \times C_p^{UO2} + x_{NpO_2} \times C_p^{NpO2} \tag{S15}$$

Where C_p^{UO2} and C_p^{NpO2} are heat capacity of pure UO_2 and NpO_2. x_{UO_2} and x_{NpO_2} are the fraction of UO_2 and NpO_2.

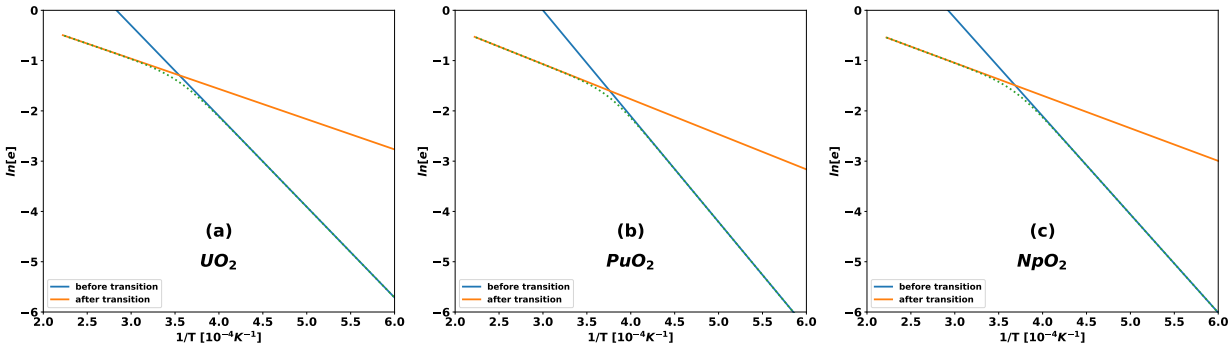

Figure S1: Defect concentration as function of 1/T for (a) UO_2, (b) PuO_2 and (c) NpO_2

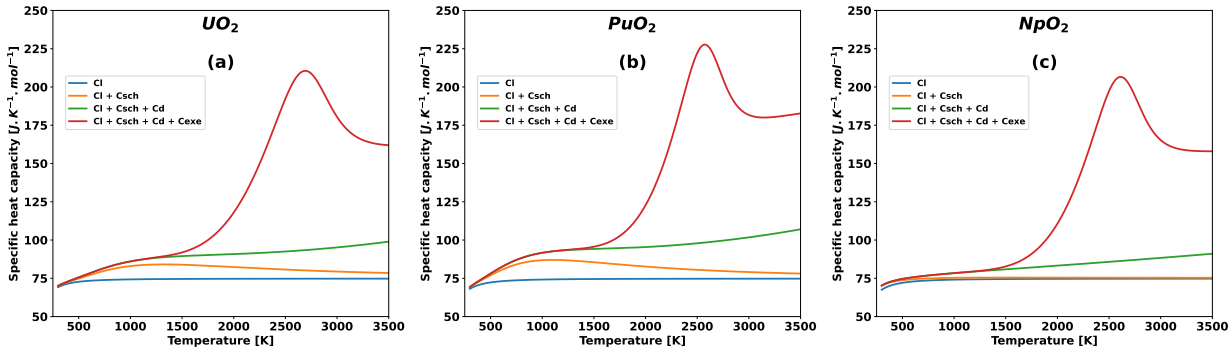

Figure S2: A comparison of specific heat (C_p) of pure (a) UO_2, (b) PuO_2, and (c) NpO_2 and the contribution of different components obtained from the model developed by Kato et al.[10] (line).

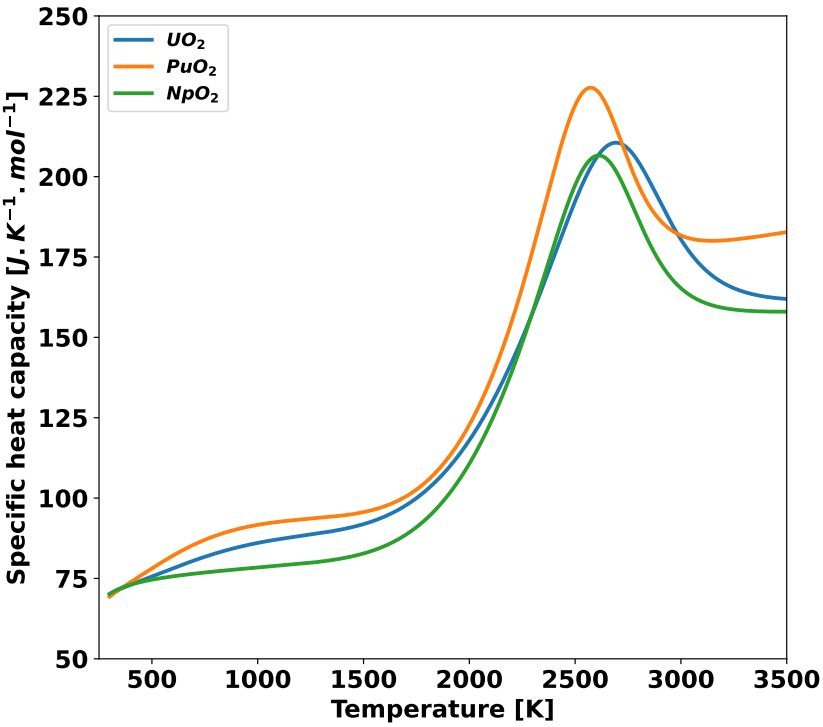

Figure S3: A comparison of specific heat (C_p) of pure UO_2, PuO_2, and NpO_2 and the contribution of different components obtained from the model developed by Kato et al.[10] (line).

References

(1) Cooper, M. W. D.; Rushton, M. J. D.; Grimes, R. W. A many-body potential approach to modelling the thermomechanical properties of actinide oxides. *J. Phys.: Condens. Matter* **2014**, *26*, 105401.

(2) Liu, X.-Y.; Cooper, M. W. D.; McClellan, K. J.; Lashley, J. C.; Byler, D. D.; Bell, B. D. C.; Grimes, R. W.; Stanek, C. R.; Andersson, D. A. Erratum: Molecular Dynamics Simulation of Thermal Transport in UO_2 Containing Uranium, Oxygen, and Fission-Product Defects [Phys. Rev. Applied 6, 044015 (2016)]. *Phys. Rev. Appl.* **2017**, *7*, 059901.

(3) Takoukam-Takoundjou, C.; Bourasseau, E.; Rushton, M. J. D.; Lachet, V. Optimization

of a new interatomic potential to investigate the thermodynamic properties of hypo-stoichiometric mixed oxide fuel U1yPuyO2x. *Journal of Physics: Condensed Matter* **2020**, *32*, 505702.

(4) Yamashita, T.; Nitani, N.; Tsuji, T.; Kato, T. Thermal expansion of neptunium-uranium mixed oxides. *Journal of Nuclear Materials* **1997**, *247*, 90–93, Thermodynamics of Nuclear Materials.

(5) Yamashita, T.; Muto, H.; Tsuji, T.; Nakamura, Y. Thermal expansion of neptunium–plutonium mixed oxides. *Journal of Alloys and Compounds* **1998**, *271-273*, 404–407.

(6) Nishi, T.; Itoh, A.; Takano, M.; Numata, M.; Akabori, M.; Arai, Y.; Minato, K. Thermal conductivity of neptunium dioxide. *Journal of Nuclear Materials* **2008**, *376*, 78–82.

(7) Kruger, O. L.; Savage, H. Heat capacity and thermodynamic properties of plutonium dioxide. *The Journal of Chemical Physics* **1968**, *49*, 4540–4544.

(8) Serizawa, H.; Arai, Y.; Takano, M.; Suzuki, Y. X-ray Debye temperature and Grüneisen constant of NpO2. *Journal of Alloys and Compounds* **1999**, *282*, 17–22.

(9) Serizawa, H.; Arai, Y.; Nakajima, K. The estimation of the heat capacity of NpO2. *The Journal of Chemical Thermodynamics* **2001**, *33*, 615–628.

(10) Kato, M.; Oki, T.; Watanabe, M.; Hirooka, S.; Vauchy, R.; Ozawa, T.; Uwaba, T.; Ikusawa, Y.; Nakamura, H.; Machida, M. A science-based mixed oxide property model for developing advanced oxide nuclear fuels. *Journal of the American Ceramic Society* **2024**, *107*, 2998–3011.

(11) Konings, R.; Beneš, O. The heat capacity of NpO2 at high temperatures: The effect of oxygen Frenkel pair formation. *Journal of Physics and Chemistry of Solids* **2013**, *74*, 653–655.